Quantitation of Membrane Receptor Distributions by Image Correlation Spectroscopy: Concept and Application

Nils O. Petersen,* Pia L. Höddelius,‡ Paul W. Wiseman,* Olle Seger,§ and Karl-Eric Magnusson¶
*Department of Chemistry, the University of Western Ontario, London, Ontario, Canada N6A 5B7; Departments of ‡Cell Biology, §Electrical Engineering, and ¶Medical Microbiology, Faculty of Health Sciences, the University of Linköping, Linköping, Sweden

ABSTRACT Measurement of receptor distributions on cell surfaces is one important aspect of understanding the mechanism whereby receptors function. In recent years, scanning fluorescence correlation spectroscopy has emerged as an excellent tool for making quantitative measurements of cluster sizes and densities. However, the measurements are slow and usually require fixed preparations. Moreover, while the precision is good, the accuracy is limited by the relatively small amount of information in each measurement, such that many are required. Here we present a novel extension of the scanning correlation spectroscopy that solves a number of the present problems. The new technique, which we call image correlation spectroscopy, is based on quantitative analysis of confocal scanning laser microscopy images. Since these can be generated in a matter of a second or so, the measurements become more rapid. The image is collected over a large cell area so that more sampling is done, improving the accuracy. The sacrifice is a lower resolution in the sampling, which leads to a lower precision. This compromise of precision in favor of speed and accuracy still provides an enormous advantage for image correlation spectroscopy over scanning correlation spectroscopy. The present work demonstrates the underlying theory, showing how the principles can be applied to measurements on standard fluorescent beads and changes in distribution of receptors for platelet-derived growth factor on human foreskin fibroblasts.

INTRODUCTION

Fluorescence microscopy studies of membrane proteins, particularly receptors to lectins, hormones, and other signal transducers, have in the last two decades provided vivid images of distributions and redistributions of these proteins as a function of activation (Bourguignon and Bourguignon, 1984; Schlessinger et al., 1978; Barak and Webb, 1981; Haigler et al., 1978; Hillman and Schlessinger, 1982). Quantitative measurements of the rate of diffusion and the fractions of mobile receptors have aided in understanding the influence of, and the interactions with, other membrane-associated components and the cytoskeleton in the cell (Elson and Reidler, 1979; Ljungquist et al., 1989; Ljungquist-Höddelius et al., 1991). The combination of biophysical and biochemical experiments has provided significant insight into the mechanisms of action of receptors in signal transduction (Schlessinger, 1988). Nevertheless, attempts to quantitate the receptor distribution in terms of their state of aggregation, or changes in the same, have been difficult. Electron microscopy has provided evidence for associations of membrane proteins in clusters, but sampling and time resolutions have been difficult to control (McKanna et al., 1979; Boonstra et al., 1985; Van Belzen et al., 1988). It has also been extremely hard to provide a firm correlation between the amount of ligand added and the extent of binding as detected by electron microscopy (Van Belzen et al., 1988). Fluorescence energy transfer methods have in some cases provided excellent evidence for protein-protein associations on a dynamic basis but have been less successful in giving quantitative evidence for the extent of participation of proteins and the size of the clusters involved (Schreiber et al., 1980; Dale et al., 1981).

The most successful set of quantitative measurements has been obtained by scanning fluorescence correlation spectroscopy (Petersen, 1984, 1986; Petersen et al., 1986). Initially developed as a concentration correlation spectroscopy method for determining molecular weights of DNA fragments in solution (Weissman et al., 1976; Weissman, 1981), it was soon adapted as fluorescence correlation spectroscopy for measurements of diffusion or directed flow (Elson and Magde, 1974; Magde et al., 1974; Magde et al., 1978). The potential for measurements of aggregation was also recognized and documented (Magde et al., 1978). The specific application to cell membranes was for years frustrated by the relatively slow dynamic processes of cell membranes. Diffusion was too slow to provide the required fluctuations in fluorescence intensity on a time scale that could be measured.

Scanning fluorescence correlation spectroscopy provided the solution by measuring the intensity fluctuations as a function of position rather than time (Petersen, 1984, 1986; Petersen et al., 1986). By the ergodic principle, the two approaches are identical as long as sufficient data are collected (McQuarrie, 1976). A very precise translation of the cell under a laser beam in a fluorescence microscope produces an intensity profile as a function of position across the cell. Correlation analysis of the magnitude of the fluctuations yields the number of fluorescent entities, or clusters, present per unit area. In conjunction with the total fluorescence intensity, which reflects the total number of receptors in the same area, it is possible to estimate the corresponding number of receptors per cluster.

Concanavalin A binds to high- and low-affinity sites on the surface of fibroblasts (Feller et al., 1977). Approximately 1%

Received for publication 23 February 1993 and in final form 26 May 1993.
Address reprint requests to Dr. Nils O. Petersen.

0006-3495/93/09/1135/12 $2.00

of the sites are of high affinity, with an affinity constant 1000 times greater than the remaining 99%. Scanning correlation spectroscopy measurements were performed on cells labeled with concanavalin A at concentrations covering three orders of magnitude. These experiments revealed that at low concentration the lectin bound to a small population of receptors distributed as monomers across the surface, whereas at high concentration the majority of the lectin is bound to a few clusters with a large number of receptors (St-Pierre and Petersen, 1990). It appears that the high-affinity sites correspond to monomeric receptors, whereas the low-affinity ones are present in large aggregates.

In more recent work (St-Pierre and Petersen, 1992), the distribution of antibodies specific for the epidermal growth factor receptor was measured on A431 cells. The concentration dependence clearly showed that all of the antibody bound to receptors with a single affinity, as expected for the antibodies employed (IgG29.1 and IgG528) (Yarden et al., 1985; Kawamoto et al., 1983). Further analysis showed that the epidermal growth factor receptors are distributed evenly among clusters with an average of 130 receptors per cluster. The cluster density is between 7 and 8/μm^2.

While scanning correlation spectroscopy evidently is able to provide detailed estimates of receptor distributions, the technique requires considerable time, about 2–4 min/scan on a cell. To achieve sufficient accuracy, several measurements on many cells are needed. Moreover, the technique requires specialized equipment, so only a few laboratories have even attempted these measurements.

The very recent advance of confocal scanning laser microscopy (CSLM) provides an opportunity to improve the aggregation measurements in a number of ways: (*a*) confocal microscopes can collect images in a matter of seconds, so the time frame of experiments is improved; (*b*) the confocal image may contain data from the entire cell, or in some cases from several cells simultaneously, so that a single image provides more information than several single scans; (*c*) confocal microscopes are becoming common tools in a number of laboratories, so aggregation measurements can potentially become routine. The price one pays for these advantages is a decrease in the resolution and a corresponding loss of precision.

In the present manuscript, we describe the concept of image correlation spectroscopy (ICS), advance the necessary theoretical framework, illustrate the theory using ICS measurements of standard fluorescent beads, and provide an example of a biological application to the measurement of the distribution and redistribution of β receptors to the platelet-derived growth factor (PDGF) on AG 1523 human foreskin fibroblasts.

MATERIALS AND METHODS

Fluorescent beads of two different diameters were used to make samples for viewing on a confocal microscope. Fluoresbrite microspheres with radii of 0.44 μm (s = 0.015 μm) and 0.026 μm (s = 0.0015 μm) were obtained from Polysciences, Inc. (Warrington, PA) (catalog nos. 15702 and 17149, respectively). Samples contained beads of only one size. The fluorescent spheres were suspended in mounting medium between two 18-mm coverslips. The coverslip assemblies were then attached to standard optical microscope slides using the same mounting medium.

The bead samples were examined under general epifluorescence illumination using a Nikon microscope with a 60× oil immersion lens (numerical aperture, 1.40) and filters appropriate for fluorescein. Confocal scanning laser microscopy was performed on a Biorad MRC 600 confocal microscope (Biorad Microscience, Ltd., Hertfordshire, England). Illumination was from a 25-mW argon-ion laser at 488 nm, and the pinhole aperture was opened to 5.8 mm (setting 12 on the Biorad Vernier scale). Images were collected with one scan or as averaged scans. All of the images were collected as square images with 512 × 512 pixels and a zoom factor of 8, which corresponded to a pixel resolution of 0.040 μm in the x and y directions.

The e^{-2} laser beam radius, a necessary parameter for the fitting of the correlation functions (see Theory), was measured using the gold edge method (Schneider and Webb, 1981; Firester et al., 1977). Briefly, the method entails sweeping a focused laser beam across a sharp gold edge and collecting the resulting signal by reflectance optics. The resulting signal profile represents the integrated intensity profile. If the transverse intensity profile of the laser is gaussian, the collected signal profile will in fact be the cumulative gaussian distribution function. Consequently, plotting the signal profile using a probability scaled ordinate will yield a straight line when the laser beam intensity profile is gaussian.

The "length profile" feature of the Biorad MRC 600 was used to collect intensity profiles from images of gold edges. Care was exercised in setting the black level and gain to ensure a small, but measurable background and to prevent saturation. The signal intensity profiles were plotted with the fluorescent intensity on a probability-scaled ordinate and scan distance on the abscissa in order to facilitate a first-order linear regression on the data. The e^{-2} radius was determined from the difference between the scan distances corresponding to the 15.9% (+1 σ) and 84.1% (−1 σ) intersections with the regression line.

Monoclonal antibodies directed specifically toward the β receptor of platelet-derived growth factor (PDGFR-β2) (Rönnstrand et al., 1988) were kindly provided by Dr. C. H. Helldin of the Ludwig Institute for Cancer Research (Uppsala, Sweden). Briefly, the antibody binds to the extracellular part of porcine and human PDGF receptor, does not inhibit ^{125}I-PDGF binding to the receptor, but does precipitate the receptor in suspensions. On cells, the antibody induces patching. A FITC-labeled goat-anti-mouse IgG specific for the Fc portion of the mouse monoclonal antibody (catalog no. F-5387; Sigma, St. Louis, MO) was used as a second antibody in order to visualize the PDGFR-β2 when bound to the receptors.

Human dermal fibroblasts (AG 1523) were maintained at 37°C in a humidified incubator at 5% CO_2 (type CO_2-AutoZero; Heraeus, Hanau, Germany) in Eagle's minimum essential medium (Gibco, Ltd., Paisley, Scotland) with 10% fetal calf serum and a penicillin (50 IU/ml)-streptomycin (50 μg/ml) mixture. For selected experiments the cells were subcultured on 12-mm-diameter glass coverslips in petri dishes in the same medium to give "normal" cells. Some cells were switched to medium MCDB 105 (Gibco, Ltd.) with 1 mg/ml serum albumin after 3 days to give "starved" cells, that is, serum-free growth conditions. In all cases the cells were used for experiments on the fifth day of subculture.

At the times indicated in the various experiments, cells were fixed in a 1% paraformaldehyde solution in a Krebs-Ringer phosphate buffer (at pH 7.3 with 1 mM calcium and magnesium ions and 10 mM glucose) for 20 min at room temperature. The sample was washed three or four times prior to subsequent use. At the appropriate times, the cells were treated with PDGFR-β2 at 50 μg/ml for 30 min, followed by extensive washing with Krebs-Ringer phosphate buffer. The final step was labeling with FITC anti-mouse antibody at 1:20 dilution for 30 min at room temperature. All incubations prior to fixing with paraformaldehyde were conducted at 37°C, while all incubations following fixing were performed at room temperature.

Samples were viewed by phase contrast and under general epifluorescence illumination in a Nikon microscope using filters appropriate for fluorescein at magnifications ranging from 250 to 1000. Confocal scanning laser microscopy was performed with a Phoibos 1000 microscope (Molecular Dynamics, Sunnyvale, CA). Illumination was from a 25-mW argon ion laser

at 488 nm. Detection was usually through a 100-μm-diameter pinhole and with a 100× (numerical aperture, 1.4) objective. The laser intensity was adjusted to minimize photobleaching, and the photomultiplier sensitivity was adjusted to provide a clear fluorescence image without saturation at any one pixel. In most cases a series of three to five images was added to improve signal to background. All regions of cells were selected so that most of a region was within the focal plane of the microscope and the scanning plane.

Images obtained on the Phoibos 1000 were all obtained at the greatest possible magnification and resolution corresponding to using a 100× objective and an image with 256 × 256 pixels. This gives a pixel resolution of 0.1 μm in either direction. The laser beam is measured indirectly in the correlation analysis and was found to be four pixels, or around 0.8 μm, in the e^{-2} diameter.

Correlation analysis was performed in either of two ways for the biological experiments: (*a*) by direct calculation of the correlation function in two dimensions and (*b*) by two-dimensional Fourier transformation of the image, followed by complex conjugate multiplication of the transform by itself and finally reverse Fourier transformation (see Theory). The second approach permits easy filtering, and in many cases a gaussian filter was superimposed to minimize edge effects. Computer analyses were performed on a SUN work station at the Technical University of Linköping (Linköping, Sweden). The second method of calculating the autocorrelation function was used for all of the fluorescent bead analyses; however, no data filters were applied. These calculations were carried out on a VAX 6430 mainframe computer at the Computing and Communications Services of the University of Western Ontario (London, ON, Canada).

All confocal microscope images were printed on a Sony video printer. Correlation functions were presented and drawn with the three-dimensional graphics program Graftool (3-D Visions, Torrance, CA) or with Sigmaplot 5.0 (Jandel Scientific, San Rafael, CA).

THEORY

Correlation spectroscopy entails calculation of the autocorrelation function, $G(\tau)$, of a randomly varying function $i(t)$. This may be done in the time domain as

$$G(\tau) = \langle i(t)i(t + \tau)\rangle \tag{1}$$

where the angle brackets, $\langle\ \rangle$, indicate an integration over all time. A properly normalized autocorrelation function, $g(\tau)$, may be obtained by using

$$\delta i(t) = \frac{i(t) - \langle i(t)\rangle}{\langle i(t)\rangle} \tag{2}$$

which therefore yields

$$g(\tau) = \langle \delta i(t)\delta i(t + \tau)\rangle = \frac{\langle i(t)i(t + \tau)\rangle - \langle i(t)\rangle^2}{\langle i(t)\rangle^2} = \frac{G(\tau)}{\langle i(t)\rangle^2} - 1 \tag{3}$$

Correspondingly, the autocorrelation function may be calculated in the spacial domain, as in scanning correlation spectroscopy (St-Pierre and Petersen, 1990), by

$$g(\xi) = \langle \delta i(x)\delta i(x + \xi)\rangle \tag{4}$$

When the data consist of a set of N discrete points, the averaging is performed as sums, that is, the autocorrelation function is calculated by

$$g(\xi) = \frac{(1/N)\sum_{k=1}^{N} i(k)i(k + \xi)}{[(1/N)\sum_{k=1}^{N} i(k)]^2} - 1. \tag{5}$$

The significance of the autocorrelation function is that by definition, the variance of the fluctuations in the initial intensity function is equal to the value of the autocorrelation function in the limit as ξ vanishes:

$$\text{var } \delta i(x) = \lim_{\xi \to 0} g(\xi) = g(0). \tag{6}$$

In an ideal system, it follows from statistical mechanics (Davidson, 1962) that the variance of the fluctuations is inversely proportional to the average number of fluorescent particles in the volume being observed, so that

$$g(0) = \frac{1}{\bar{N}}, \tag{7}$$

and hence the zero value of the autocorrelation function is a direct measure of the density of the fluorescent particles.

If the random intensity variable, i, is a function of two independent variables, x and y, it is possible to define a corresponding two-dimensional autocorrelation function, $g(\xi, \eta)$:

$$g(\xi, \eta) = \langle \delta i(x, y)\delta i(x + \xi, y + \eta)\rangle, \tag{8}$$

which for a discrete set of data is calculated as

$$g(\xi,\eta) = \frac{(1/NM)\sum_{k=1}^{N}\sum_{l=1}^{M} i(k, l)i(k + \xi, l + \eta)}{[(1/NM)\sum_{k=1}^{N}\sum_{l=1}^{M} i(k, l)]^2} - 1. \tag{9}$$

Now the variance of the random function is equal to the value of the correlation function in the limit where both ξ and η vanish. Thus we conclude that the density of the fluorescent particles can be measured by the magnitude of $g(0,0)$, that is,

$$g(0, 0) = \lim_{\xi \to 0}\lim_{\eta \to 0} g(\xi, \eta) = \frac{1}{\bar{N}}. \tag{10}$$

The traditional definition of the variance

$$\text{var } \delta i(t) = \langle [\delta i(t)]^2\rangle - \langle \delta i(t)\rangle^2 = \frac{\langle i(t)^2\rangle - \langle i(t)\rangle^2}{\langle i(t)\rangle^2} \tag{11}$$

cannot be used in these calculations since the evaluation will include a dominant contribution from uncorrelated noise. It is therefore always necessary to calculate the autocorrelation function and estimate the variance from the extrapolation of the autocorrelation function to the zero value. The autocorrelation function can be calculated directly as indicated by Eq. 9. This is computationally tedious but gives directly the appropriately normalized function. Alternatively, one can calculate the autocorrelation function from the Fourier transform of the power spectrum of the data, which in turn is calculated as the product of the Fourier transform of the original random function and its complex conjugate

$$G(\xi, \eta) = \mathcal{F}^{-1}([\mathcal{F}(i(x, y))] * [\mathcal{F}^*(i(x, y))]. \tag{12}$$

Because of fast Fourier transform computer algorithms, this

approach is rapid and allows for facile filtering of the data if needed. However, extreme care must be exercised in ensuring that Fourier normalization is carried through correctly. Otherwise, the magnitude of the calculated correlation function is incorrect and consequently the interpretation of $g(0, 0)$ is wrong. The properly normalized correlation function, $g(\xi, \eta)$, is obtained by dividing $G(\xi, \eta)$ by the square of the mean intensity and then subtracting 1.

Estimates of $g(0, 0)$ values can be made by fitting the two-dimensional correlation function to a two-dimensional gaussian function determined by the transverse intensity profile of the laser beam used in the experiment:

$$g(\xi, \eta) = g(0, 0)e^{-(\xi^2+\eta^2)/w^2}, \quad (13)$$

where w is the e^{-2} radius of the laser beam. Since the image is restricted in dimension, it is frequently difficult to sample enough data to allow the correlation function to vanish at large correlation distances. The resulting dc component must therefore be included in the fitting procedure through a g_0 value:

$$g(\xi, \eta) = g(0, 0)e^{-(\xi^2+\eta^2)/w^2} + g_0. \quad (14)$$

Alternatively, estimates of $g(0, 0)$ can be made by fitting the autocorrelation function data along either the ξ or the η axis to a one-dimensional analog of Eq. 14. This permits several independent ways of assessing the magnitude of $g(0, 0)$ for comparisons.

In general, the fit is made using the three parameters $g(0, 0)$, g_0, and w. Only data that yield a beam width w within 30% of the known or measured value for the particular microscope system are retained. Smaller values of w are indicative of very sharp edges or unusually large noise levels in particular pixels. Larger values of w appear if there are patches that are large compared to the beam size. At low densities of clusters, even small patches, which act as point sources, will appear as large as the beam in an image since the beam is the ruler by which the patches are measured.

RESULTS AND DISCUSSION

Beam measurements

As is explained in the theory section of this paper, the e^{-2} laser beam radius is one of the autocorrelation function fitting parameters. The radius can be obtained indirectly from the fitting procedure; however, the beam must be measured independently if the beam radius is to be used as the criterion to determine whether or not a desired image provides a physically meaningful $g(0, 0)$ value. The e^{-2} laser beam radius is measured via the gold edge method to be 0.31 μm (s = 0.04 μm) for the Biorad MRC 600 CLSM with a 60× oil immersion lens and a full zoom factor of 8. Fig. 1 vividly illustrates how the gold edge technique can be used to accurately determine the size of a submicron focused laser beam. Fig. 1 *D* also shows the effective beam radius as a function of pinhole aperture setting for the Biorad microscope. It is evident that a small pinhole restricts the beam size on this instrument. A large beam profile in the focal plane is desired, since the laser beam is the correlator in this type of experiment. For this reason a large pinhole aperture was used for all measurements.

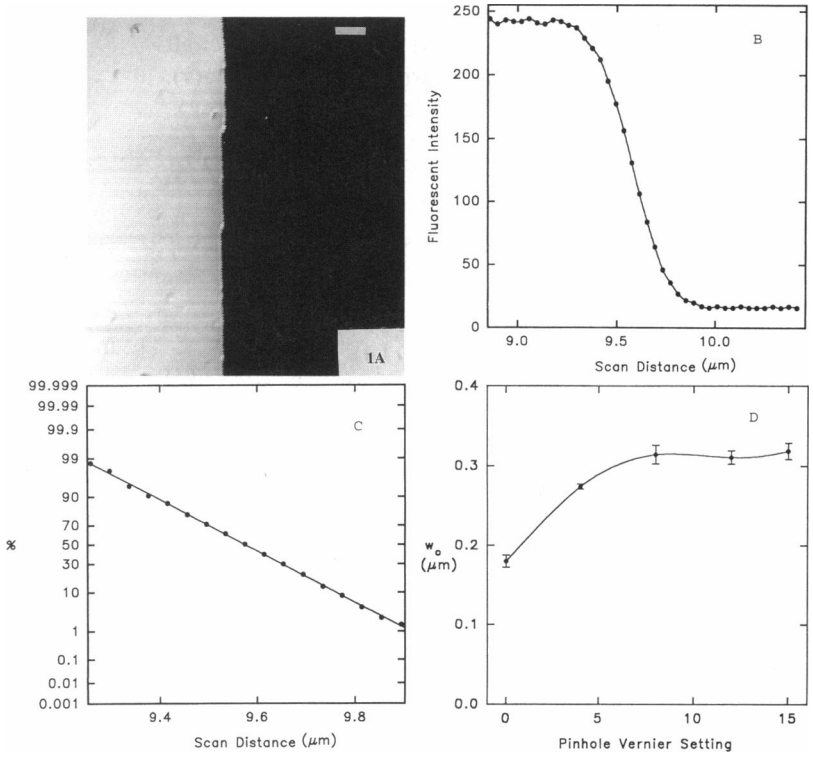

FIGURE 1 Determination of submicrometer laser beam radius using the gold edge method. (*A*) confocal image of a sharp gold edge as measured using reflectance optics on a CSLM. The scale bar indicates 2 μm. (*B*) intensity profile across a line perpendicular to the gold edge. Note the characteristic shape of the cumulative gaussian distribution. (*C*) portion of the same intensity profile data, normalized according to percentage intensity, plotted versus a probability ordinate. The beam radius is obtained using the linear regression equation calculated for the data. (*D*) effect of pinhole size on the effective beam radius for a BioRad MRC 600 CSLM. It is evident that lower settings of the pinhole aperture restrict the size of the laser beam. It is desirable to have as large a beam as possible for ICS measurements. The error bars represent the SEM for the data.

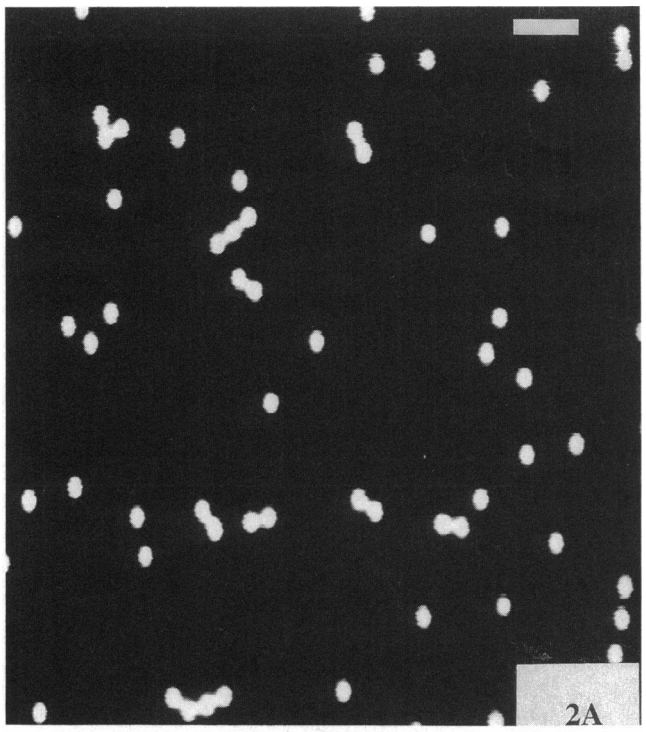

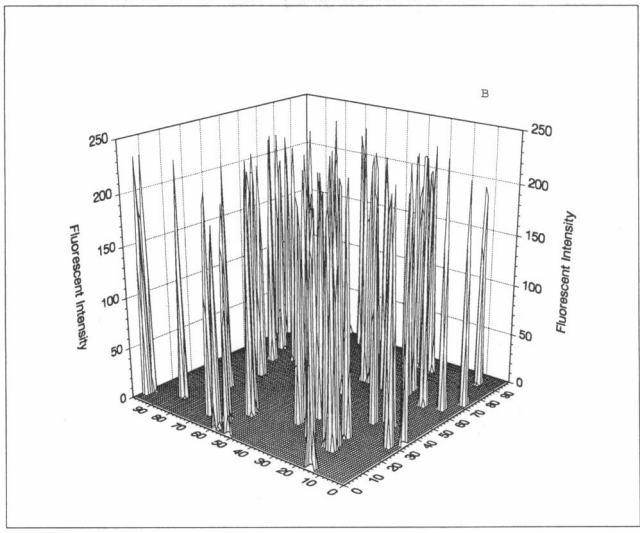

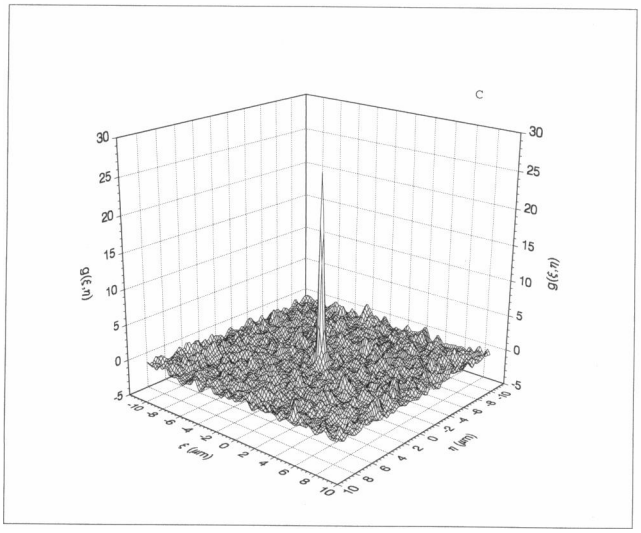

Experiments with beads

Fig. 2 depicts a confocal image of the large (0.44 μm nominal radius) fluorescent beads, with a corresponding three-dimensional graph of fluorescent intensity as a function of pixel position and the autocorrelation function calculated for the image. Due to memory limitations of the three-dimensional plotting program, only 100 × 100 points could be represented in the graphs, so the two plots do not represent the full resolution of the data. The surface plots were constructed by sampling every fifth point in the 512 × 512 image and autocorrelation data sets. A direct count of the microspheres indicates that there are 70 fluorescence-emitting entities in the image. Beads that are only partially visible at the edges are included in the count because they will contribute to the amplitude of the autocorrelation function; moreover, there are three beads in the data set that were cut off by the video printer and cannot be seen in Fig. 2.

Fig. 3 contains full resolution (central 64 × 64 points) results of the two-dimensional fit to the correlation function plotted in the positive, positive quadrant with the raw correlation data in the other three quadrants. Data points that were within a 0.64-μm radius (two times the laser beam radius) of the center of the autocorrelation matrix were included in the two-dimensional fit. Also included in the figure are one-dimensional fits to the data along the two independent correlation axes. Eq. 15 gives the functions to which the data are fit for the one-dimensional analyses:

$$g(\xi, 0) = g(0, 0)e^{-\xi^2/w^2} + g_{0\xi}$$
$$g(0, \eta) = g(0, 0)e^{-\eta^2/w^2} + g_{0\eta}. \quad (15)$$

These plots clearly show the gaussian profile of the correlation data and indicate that the beam does have a gaussian transverse intensity profile. The laser beam radius obtained from the two-dimensional fit is 0.27 μm, and this compares favorably with the measured radius of 0.31 μm, indicating that the information contained in the autocorrelation function is physically meaningful.

The $g(0, 0)$ value obtained from the two-dimensional least-squares fit is 25.6, and this value is inversely proportional to the average number of fluorescent beads in the observation area. The number of beads in the image can be calculated theoretically using the $g(0, 0)$ value, the image area, and the laser beam area. The latter is determined from

FIGURE 2 Confocal image and correlation function of large (0.44 μm radius) fluorescent beads. (*A*) 512 × 512 pixel confocal image of fluorescein-labeled microspheres, with a pixel size of 0.040 μm. The image was obtained using a BioRad MRC 600 CSLM with a pinhole Vernier scale set to 12. The scale bar represents 2 μm. (*B*) representation of the image with the fluorescent intensity plotted as a function of pixel position. To facilitate the three-dimensional graphical representation, the resolution of the points in the plot is only one-fifth that of the original image. (*C*) plot of the raw correlation function data as a function of spatial lag in the two independent image directions. The correlation function is calculated from the entire image data set, although this graph presents the data at one-fifth resolution.

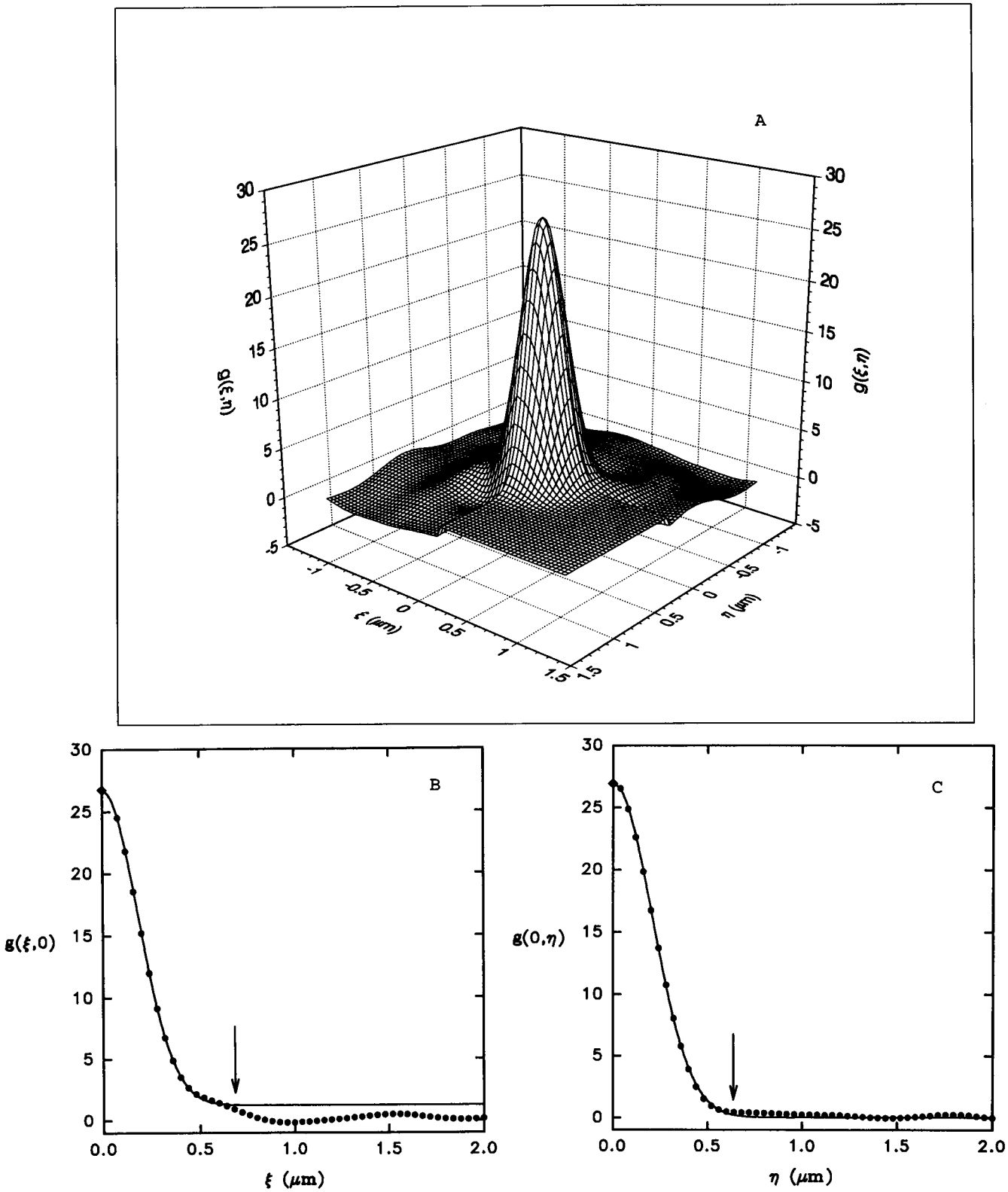

FIGURE 3 Correlation analysis of image in Fig. 2. (*A*) two-dimensional fit to the raw correlation data. The fit data are seen in the facing quadrant, and the raw correlation data are displayed in the other three. Equation 14 gives the functional form to which the data are fit. The figure displays the central 64 × 64 data channels at full resolution. (*B*) correlation data and one-dimensional fit along the ξ independent spatial lag axis. The circular data points are the raw data from the correlation function calculation, and the solid line represents the functional fit to the data. The diamond point on the ordinate shows the sum of the $g(0,0)$ value and the offset. The arrow indicates the last data point included in the fit. (*C*) correlation data and one-dimensional fit along the η independent spatial lag axis. The symbols used are as described for *B*. Equation 15 gives the functional form for the one-dimensional fits.

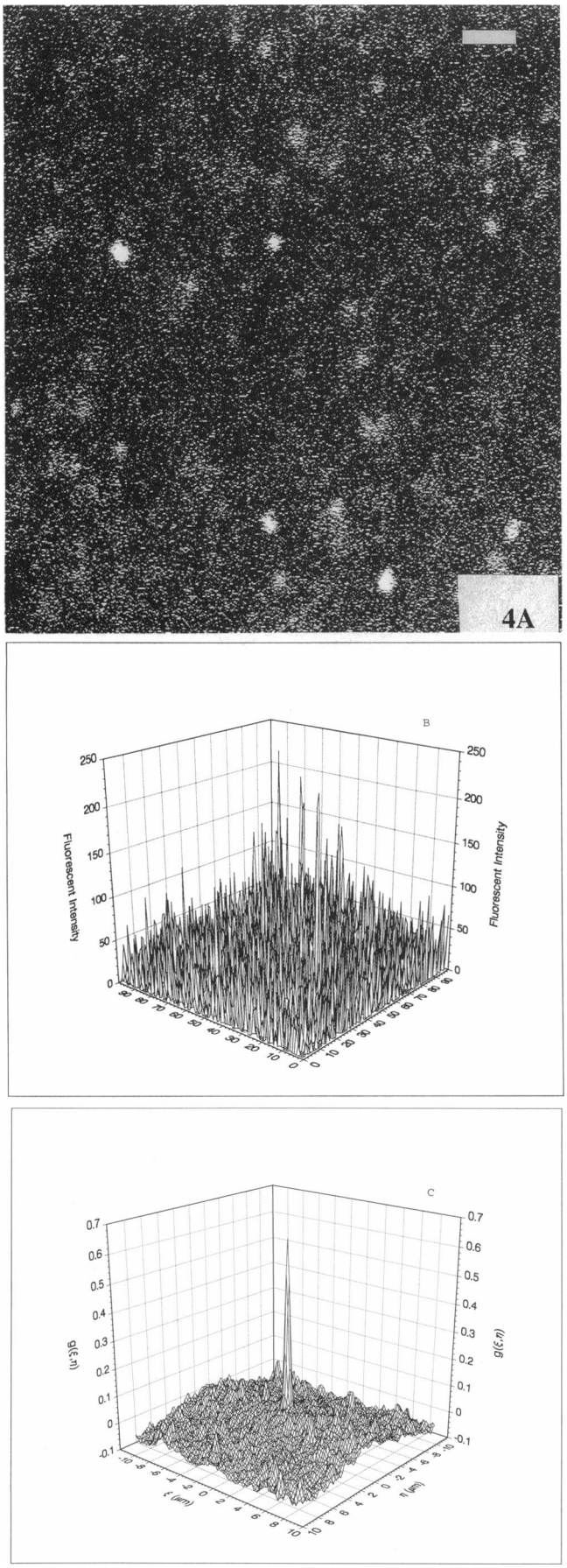

the value of the beam radius obtained from the fit, 0.27 μm in this case:

$$\text{No. of beads} = \frac{\text{Image area}}{g(0,0)\pi w_0^2} = \frac{[(512)(0.040\ \mu\text{m})]^2}{25.7\pi(0.27\ \mu\text{m})^2} = 71. \quad (16)$$

The value obtained from the correlation analysis agrees well with the actual count of the number of beads (count = 70) in this image. Correlation analyses of four different images of the large beads yielded bead counts that were all within 4% of visual bead counts. This provides experimental confirmation of the theoretical relation between the correlation function amplitude and the occupation number. It also demonstrates that the $1/\bar{N}$ relation holds for a system with high signal-to-noise ratio even when the fluorescent entities are of a size comparable to the laser beam spot size.

Fig. 4 shows a confocal image collected from a sample of the small (0.026 μm nominal radius) fluorescent microspheres, the fluorescence intensity plotted versus pixel position, and the raw autocorrelation function for this image. This image was obtained in one scan and shows much more background noise than the large bead image. The plot of the autocorrelation function does not include the central noise peak because it was excluded by virtue of the limited sampling of the correlation data set.

The results of a correlation analysis are depicted in Fig. 5. The two-dimensional fit shows noise in the first lag channel in ξ. Noise repeatedly appeared in this channel for autocorrelation functions calculated for images obtained from the Biorad CLSM. This is probably due to what we term *noise bleed*. This effect should be observed if the temporal persistance of the noise is of the same order of magnitude as the time it takes the laser beam to jump one pixel position in this direction. The scanning of the laser beam across the sample in the axis corresponding to the ξ lag axis is very rapid, and there is incomplete decay of the noise signal between adjacent pixels. Autocorrelation of the noise augments the actual correlation signal in this channel, and a noise peak results. The size of noise peak in the first channel in ξ was always smaller than the noise peak in the central channel, as one would expect for this type of phenomenon. The noise point is not weighted in either one- or two-dimensional fitting and is not shown in

FIGURE 4 Confocal image and correlation function of small (0.026 μm radius) fluorescent beads. (*A*) 512 × 512 pixel confocal image of fluorescein-labeled microspheres, with a pixel size of 0.040 μm. The image was obtained with a BioRad MRC 600 CSLM with pinhole Vernier scale set to 12. The scale bar indicates a length of 2 μm. (*B*) representation of the image with the fluorescent intensity plotted as a function of pixel position. To facilitate the three-dimensional graphical representation, the resolution of the points in the plot is only one-fifth that of the original image. (*C*) plot of the raw correlation function data as a function of spatial lag in the two independent image directions. The correlation function is calculated from the entire image data set, although this graph presents the data at one-fifth resolution.

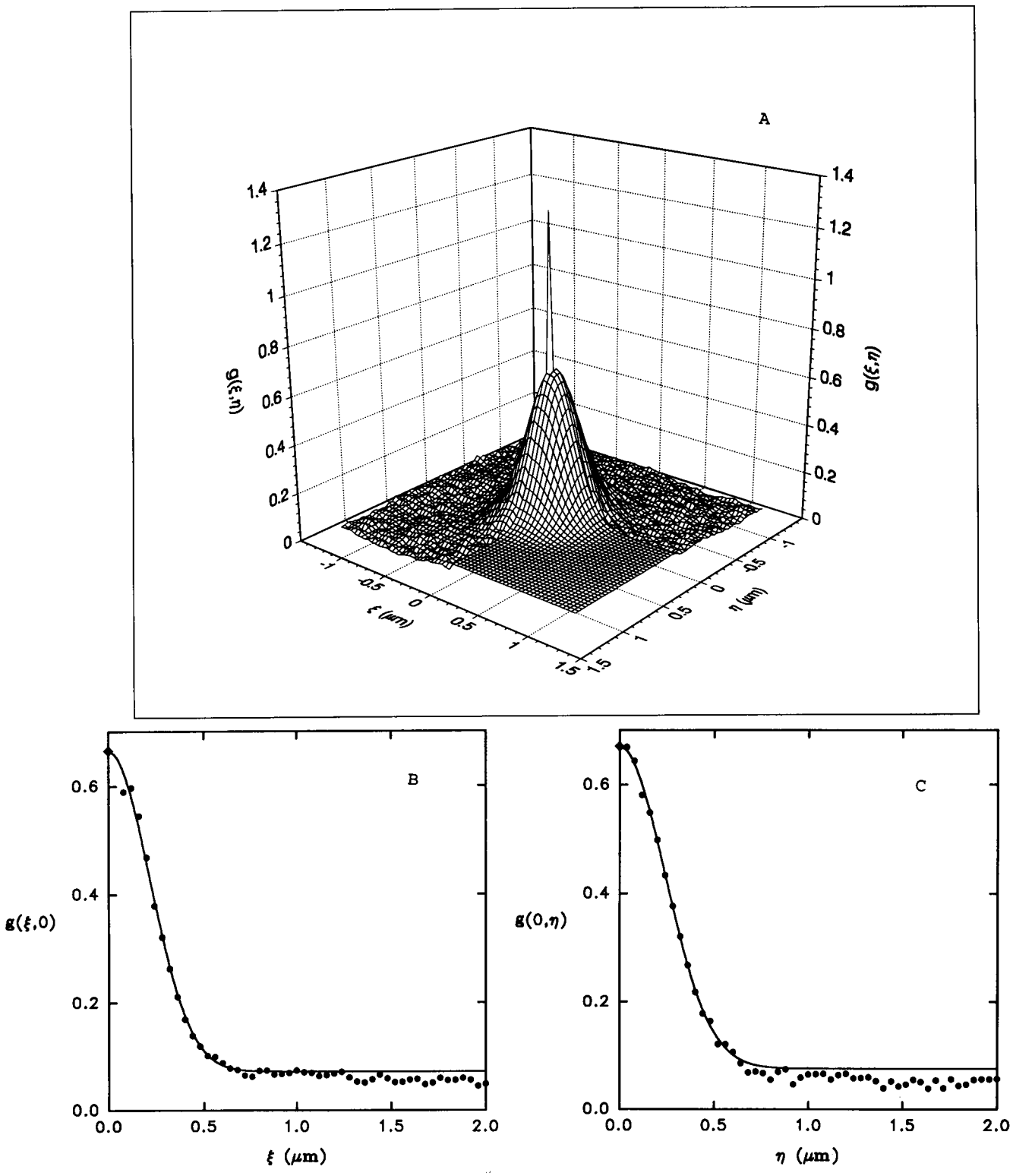

FIGURE 5 Correlation analysis of image in Fig. 4. (*A*) two-dimensional fit to the raw correlation data. The fit data are seen in the facing quadrant, and the raw correlation data are displayed in the other three. The noise peak in the first lag channel along the ξ-axis is evident. The figure shows the central 64 × 64 data channels at full resolution. (*B*) correlation data and one-dimensional fit along the ξ independent spatial lag axis. The circular data points are the raw data from the correlation function calculation, and the solid line represents the functional fit to the data. The diamond point on the ordinate shows the sum of the $g(0, 0)$ value and the offset. (*C*) correlation data and one-dimensional fit along the η independent spatial lag axis. The symbols used are as described for *B*.

the graphs of the one-dimensional fits. Again the gaussian shape of the correlation function is evident, and the laser beam radius obtained from the two-dimensional fit (0.32 μm) is very close to the measured beam radius (0.31 μm).

Calculation of the number of beads in the image using the $g(0, 0)$ value and the beam radius obtained from the two-dimensional fit (0.59 and 0.32 μm, respectively) yields a value of 2200. Although a direct count of the number of fluorescent microspheres in this image is difficult to make, it is felt that the number calculated from the correlation analysis is too large (the number of small beads should be comparable to the number of large beads in the previous image). Background fluorescence in this image gets correlated by the scanning laser beam, making it appear as if there are more fluorescent entities present, resulting in a decrease in $g(0, 0)$. The intensity of the fluorescence from the large beads (Fig. 2) is so great that little background signal is detected, and the calculated autocorrelation function is physically meaningful. Previous studies (St-Pierre and Petersen, 1990; St-Pierre and Petersen, 1992) have indicated that experiments must be performed as a series of concentrations in order to discern the effect of the background fluorescence on the amplitude of the correlation function. Averaging of several images will decrease the influence of any random noise signals but will not remove a true background fluorescence signal. Clearly, for a system with low signal-to-noise ratio, careful experimental controls must be exercised to obtain a physically meaningful number density from the autocorrelation function.

Measurements of PDGF receptor distribution changes

Antibodies directed at the receptors for platelet-derived growth factor are able to cause a redistribution of the receptors on the surface of human dermal fibroblasts. This is seen qualitatitively in Fig. 6. Cells fixed with paraformaldehyde prior to exposure to the PDGFR-β2 antibody and the FITC-labeled goat anti-mouse IgG exhibit a homogeneous fluorescence pattern when observed by conventional fluorescence microscopy (Fig. 6, *A* and *C*). In contrast, the same cells exposed to the PDGFR-β2 antibody for 1 h prior to fixing with paraformaldehyde show a more heterogeneous distribution of fluorescence (Fig. 6, *B* and *D*). It is evident that there is a change in receptor distribution as a result of the exposure to the receptor-specific antibody. The key question remains: What is the quantitative change in receptor distribution?

An example of a confocal microscope image of a human dermal fibroblast exposed to receptor-specific antibody, fixed in paraformaldehyde and labeled with the second antibody, is shown in Fig. 7*A*. Clearly, there are a large number of distinct regions on the surface that are labeled with the fluorescent antibody. Qualitatively, it appears as if there are a number of aggregates as large as 0.5 μm in diameter. However, this is misleading, as clusters that are smaller than the illuminating laser beam profile will still appear to be as large as the laser beam spot size. As the beam traverses a point-source fluorophore, it will elicit a fluorescent response across the entire beam width. The fluorescence intensity profile will depend on the intensity profile of the excitation laser, and the

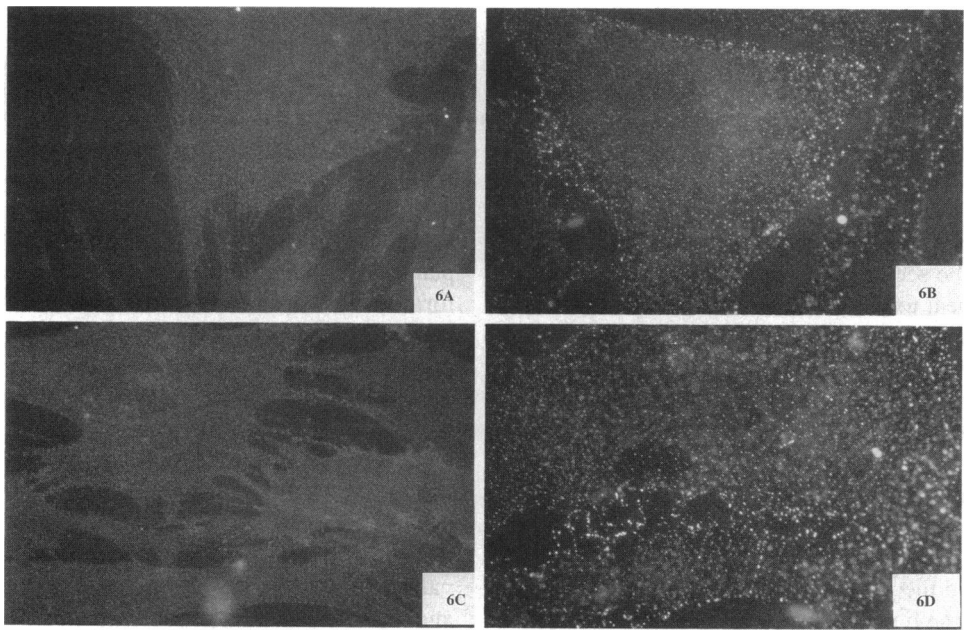

FIGURE 6 Conventional fluorescence photographs of the distribution of FITC-labeled goat-anti-mouse IgG attached to mouse monoclonal antibodies directed at the PDGF receptors on human dermal fibroblasts. (*A* and *C*) depiction of the apparently homogeneous distribution of fluorescence on the surface of cells fixed prior to exposure to the receptor specific antibody. (*B* and *D*) illustration of the redistribution of fluorescence into visible patches on the surface of cells exposed to the receptor specific antibody for 1 h prior to fixing.

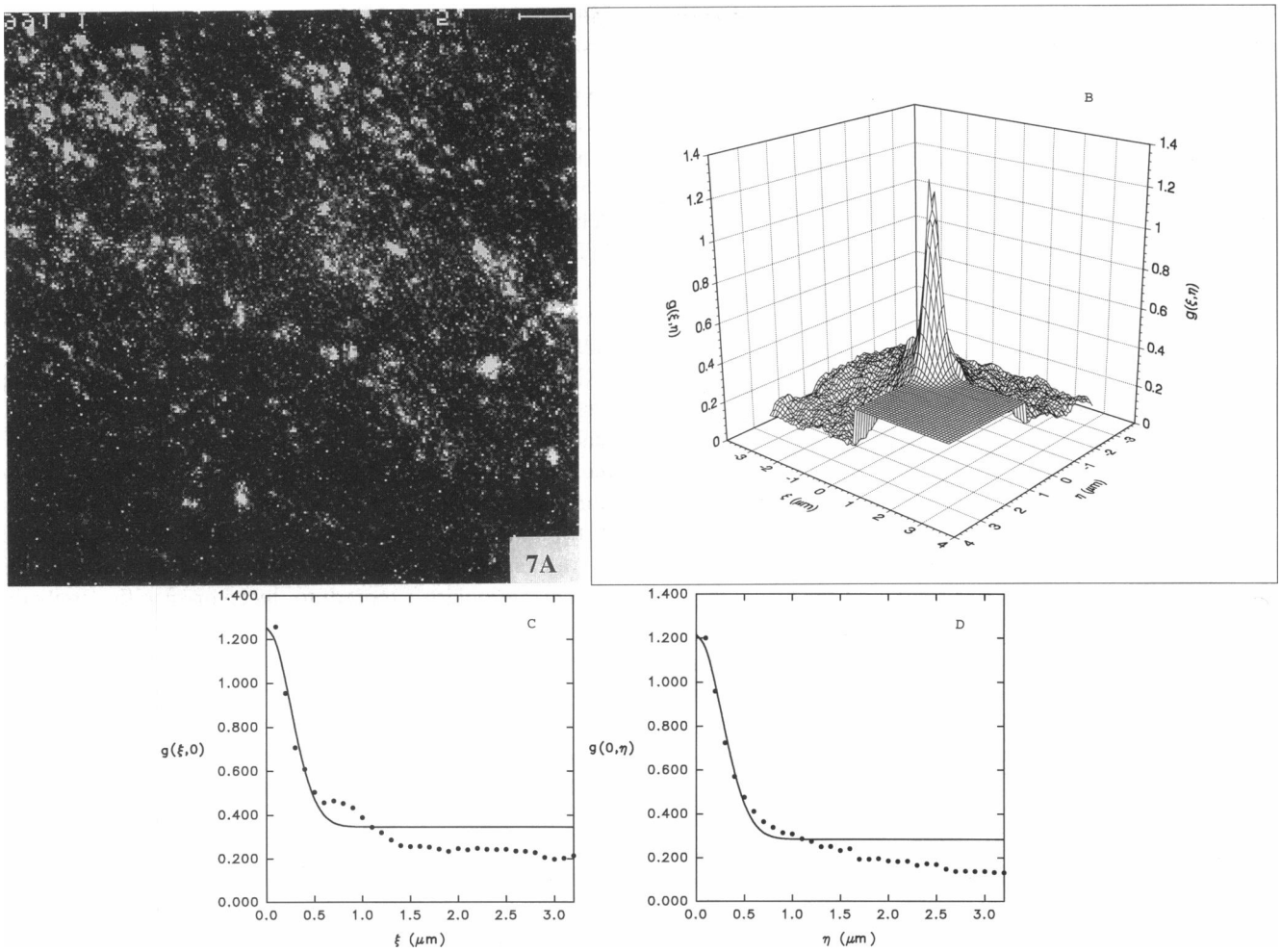

FIGURE 7 Image correlation spectroscopy of PDGF receptors on human foreskin fibroblasts. The receptors were visualized with FITC-conjugated goat anti-mouse IgG (Fc-specific) bound to monoclonal antibodies directed at the PDGF receptor (PDGF-β2). (*A*) confocal laser scanning microscope image with 256 × 256 pixels. The scale corresponds to 2 μm. None of the pixels are saturated. A total of five images were added to improve signal to background. A single, flat cell occupies better than 90% of the image. (*B*) The 64 × 64 autocorrelation function and fit derived from the image in (*A*). The calculation using Eq. 12 produces a 256 × 256 autocorrelation data matrix. This figure contains the central 64 × 64 data from this matrix with the raw correlation data in the near quadrant replaced by data obtained from a two-dimensional least-squares fit of the raw data to Eq. 14. (*C*) autocorrelation function data along the ξ lag axis (*data points*) and the best fit (*curve*) to Eq. 15. (*D*) autocorrelation function data along the η lag axis (*data points*) and the best fit (*curve*) to Eq. 15.

resulting profile will appear to be the size of the laser profile. This can clearly be seen in Fig. 4 *A*, where the small fluorescent beads appear to be as large as the illuminating beam, even though they are smaller by a factor of 6.

A two-dimensional correlation analysis of the image in Fig. 7 *A* was performed by direct calculation of the correlation function according to Eq. 12 followed by the appropriate normalization. Subsequently, least-squares fits of the data to Eqs. 14 and 15 were carried out. Fig. 7 *B* depicts the results of the two-dimensional autocorrelation analysis. The figure depicts the best-fit function in the positive lag, positive lag quandrant, and the raw autocorrelation data in the other three quadrants. The figure displays the central 64 × 64 data points from the autocorrelation matrix at full resolution. It is clear that the autocorrelation function has a maximum value at the origin (the centre of the 64 × 64 section presented) and that the function decays smoothly to a base value at the edges. The function decays to the background level within about 6–9 pixel values. This figure clearly demonstrates that the punctate pattern of fluorescence observed in Fig. 7 *A* is transformed into a smooth correlation function, as expected theoretically.

Sections of the autocorrelation function along the two independent lag axes are shown in Fig. 7 (*C* and *D*) along with the best fit to the autocorrelation data. In this case the best fit is achieved independently along the two dimensions by fits to Eq. 15.

The two-dimensional fit yielded values for $g(0, 0)$ (0.80), g_0 (0.31), and w (0.44 μm). The one-dimensional fits give values of $g(0, 0)$ [0.91 (ξ) and 0.93 (η)], g_0 (0.35 and 0.28), and w (0.36 and 0.38), which are within a few percent of each other, showing that the correlations in the two dimensions are comparable and that the laser beam is symmetric.

The beam radius for the Phoibos microscope system is determined from the two-dimensional fit to be about 4.4 pixels, which corresponds to 0.44 μm. The value of $g(0, 0)$

of 0.80 is inversely proportional to the average density of fluorescent clusters within the beam area across the cell. The beam area is $\pi w^2 = 0.61\ \mu m^2$. Thus, the average density is 2 clusters/μm^2 for this particular example. This value only provides information on the average number of fluorescent entities present; it does not allow one to deduce the size of the clusters or to determine whether there is a distribution of clusters of varying size.

The data in Fig. 7 demonstrate it is possible to get quantitative information from the confocal images of labeled receptors on cells. With careful calibrations and concentration-dependent studies it would be possible to obtain the number of receptors per cluster, as was done with scanning fluorescence correlation spectroscopy previously (St-Pierre and Petersen, 1992). Alternatively, information on the range of aggregate sizes can be obtained via high-order correlation analysis (Palmer and Thompson, 1987; Qian and Elson, 1990). For the present purpose, a comparative analysis is presented.

Table 1 summarizes the image correlation spectroscopy data obtained from a series of experiments in which cells were either fixed and exposed to receptor-specific antibody or exposed to antibody for 60 min and then fixed. The results are compared to samples in which nonspecific binding of the second, fluorescein-labeled antibody was measured in the absence of the receptor-specific antibody.

In the absence of the first antibody, the nonspecific fluorescence (which incorporates autofluorescence background from the cells) showed homogeneity to the extent that it was almost impossible to measure a correlation function above the noise. Accordingly, the beam width for these experiments could not be determined. When the cells are fixed prior to exposure to the receptor-specific antibody, the distribution of antibody is fairly homogeneous, exhibiting about 1/0.07 = 14 receptor clusters/beam area or about 33 clusters/μm^2. On the other hand, when the receptors have been exposed to the specific antibody for an hour, the correlation function increases by a factor of almost 5, corresponding to a decrease in the cluster density to about 6.7 clusters/μm^2. The effect of the receptor-specific antibody is therefore to cause aggregation of the receptors into clusters that contain almost 5 times more receptors. Unfortunately, the lack of intensity calibration in the confocal microscope currently precludes assessment of the total number of receptors labeled and therefore the exact number of receptors per cluster.

It should be noted that the accuracy of the cluster density measurement will depend on whether or not the image includes only the cell surface. In fact, the lower left-hand corner of the image in Fig. 7 *A* represents an area in which there is no cell. This is seen clearly in phase-contrast observation of the same cell and is manifested by the low total intensity in this region. The large change in fluorescent intensity at the boundary of the cell will introduce edge effect artifacts into the correlation function. A proper autocorrelation calculation should therefore be performed only on the region of the image corresponding to the true cell surface, but this is difficult because of the irregular shapes of some cells. The problem can be overcome by using the zoom feature present on most confocal microscopes to ensure that the image is produced exclusively by signal from the cell surface. If this had been performed in the present case, a slightly higher average density would have been obtained.

TABLE 1 Amplitudes of autocorrelation functions and beam widths measured on samples without (nonspecific) or fixed prior to (fix + antibody), or after (antibody + fix) exposure to receptor-specific antibodies.

Experiment	g (0,0)	$w/\mu m$
Nonspecific	<0.01	Not determined
Fix + antibody	0.07 ± 0.02	0.37
Antibody + fix	0.33 ± 0.10	0.38 ± 0.03

The uncertainty is quoted as a SEM.

CONCLUSIONS

ICS is a novel extension of scanning fluorescence correlation spectroscopy that improves upon its progenitor. The speed of data acquisition was greatly increased, and the accuracy should be improved due to the inherent sampling of more data through imaging as compared to scanning. A loss in precision results due to the smaller focal cross section and larger scanning step size of the laser used in the confocal microscope. However, the experiments performed show that meaningful data are obtained using the new technique. Moreover, ICS is more generally applicable than scanning fluorescence correlation spectroscopy because of the wide availability of confocal microscopes.

The experiments with fluorescent beads demonstrated that ICS could be used to accurately determine the density of fluorescent entities in an image, provided there is little background fluorescence. In the presence of significant background, quantitation becomes more difficult and careful controls are necessary. Immunofluorescence experiments on PDGF β2 receptors vividly demonstrated that ICS was sensitive to changes in the underlying distribution of receptors. In particular, changes in the aggregation state of the receptors were easily detected. ICS could become a powerful tool for the study of aggregation phenomena and could potentially be used by anyone with access to a confocal microscope and the appropriate computing environment. The rapid speed of image acquisition in ICS will eventually allow temporal characterization of the dynamics of biological receptor aggregation. Experiments are currently being performed to demonstrate the application of the technique to kinetic studies.

The supply of receptor antibodies and platelet-derived growth factor hormone by Dr. C. H. Helldin is gratefully acknowledged. We thank Kajsa Holmgren for invaluable assistance with the Phoibos 1000 confocal microscope and both Michael Gustafsson and Paul St-Pierre for extensive and productive discussions.

The work was supported by an operating grant from the Natural Sciences and Engineering Research Council, Canada (NOP) and by a Visiting Scientist Fellowship (K90-16V-09334-01) from the Swedish Medical Research Council (NOP) in addition to support awarded to KEM by the Swedish Medical Research Council (project 6251), the Swedish Research Council for Engineering Sciences, the Knut and Alice Wallenberg Foundation, the Erna

and Victor Hasselblad Foundation, the Magnus Bergvall Fund, the Per Eckerberg Foundation, and the Carl Trygger Scientific Foundation and the Swedish Medical Research Council (Project 4486) (PLH). PWW is a Natural Sciences and Engineering Research Council Postgradute Fellow.

REFERENCES

Barak, L. S., and W. W. Webb. 1981. Fluorescent low density lipoprotein for observation of dynamics of individual receptor complexes on cultured human fibroblasts. *J. Cell Biol.* 90:595–604.

Boonstra, J., P. van Maurik, L. H. K. Defize, S. W. de Laat, J. L. M. Leunissen, and A. J. Verkleij. 1985. Visualization of epidermal growth factor receptor in cryosections of cultured A431 cells by immuno-gold labeling. *Eur. J. Cell Biol.* 36:209–216.

Bourguignon, L. Y. W., and G. J. Bourguignon. 1984. Capping and the cytoskeleton. *Int. Rev. Cytol.* 87:195–224.

Dale, R. E., J. Novros, S. Roth, M. Edidin, and L. Brand. 1981. Application of Forster long-range excitation energy transfer to the determination of distributions of fluorescently-labelled concanavalin-A-receptor complexes at the surfaces of yeast and of normal and malignant fibroblasts. *In* Fluorescent Probes. G. S. Beddard and M. A. West, editors. Academic Press Inc., New York. 159–181.

Davidson, N. 1962. Statistical Mechanics. McGraw-Hill Book Company, Inc. New York.

Elson, E. L., and D. Magde. 1974. Fluorescence correlation spectroscopy. I. Conceptual basis and theory. *Biopolymers.* 13:1–27.

Elson, E. L., and J. A. Reidler. 1979. Analysis of cell surface interactions by measurements of lateral mobility. *J. Supramol. Struct.* 12:481–489.

Feller, M., C. Richardson, W. D. Behnke, and E. Gruenstein. 1977. High and low binding sites for concanavalin A on normal human fibroblasts in vitro. *Biochem. Biophys. Res. Commun.* 76:1027–1035.

Firester, A. H., M. E. Heller, and P. Sheng. 1977. Knife-edge scanning measurements of subwavelength focused light beams. *Appl. Optics.* 16: 1971–1974.

Haigler, H., J. F. Ash, S. J. Singer, and S. Cohen. 1978. Visualization by fluorescence of the binding and internalization of epidermal growth factor in human carcinoma cells A-431. *Proc. Natl. Acad. Sci. USA.* 75:3317–3321.

Hillman, G. M., and J. Schlessinger. 1982. Lateral diffusion of epidermal growth factor complexed to its surface receptors does not account for the thermal sensitivity of patch formation and endocytosis. *Biochemistry.* 21:1667–1672.

Kawamoto, T., J. D. Sato, A. Le, J. Polikoff, G. H. Sato, and J. Mendelsohn. 1983. Growth stimulation of A431 cells by epidermal growth factor: identification of high affinity receptors for epidermal growth factor by an anti-receptor monoclonal antibody. *Proc. Natl. Acad. Sci. USA.* 80:1337–1341.

Ljungquist, P., Å. Wasteson, and K. E. Magnusson. 1989. Lateral diffusion of plasma membrane receptors labelled with either platelet derive growth factor (PDGF) or wheat germ agglutinin (WGA) in human polymorphonuclear leukocytes and fibroblasts. *Biosci. Rep.* 9:63–73.

Ljungquist-Höddelius, P., M. Lirvall, Å. Wasteson, and K. E. Magnusson. 1991. Lateral diffusion of PDGF β-receptors in human fibroblasts. *Biosci. Rep.* 11:43–52.

Magde, D., E. L. Elson, and W. W. Webb. 1974. Fluorescence correlation spectroscopy. II. An experimental realization. *Biopolymers.* 13:29–61.

Magde, D., W. W. Webb, and E. L. Elson. 1978. Fluorescence correlation spectroscopy. III. Uniform translation and laminar flow. *Biopolymers.* 17:361–376.

McKanna, J. A., H. T. Haigler, and S. Cohen. 1979. Hormone receptor topology and dynamics: morphological analysis using ferritin-labeled epidermal growth factor. *Proc. Natl. Acad. Sci. USA.* 76:5689–5693.

McQuarrie, D. A. 1976. Statistical Mechanics. Harper & Row, New York. 554–555.

Palmer, A. G., and N. L. Thompson. 1987. Molecular aggregation characterized by high order autocorrelation in fluorescence correlation spectroscopy. *Biophys. J.* 52:257–270.

Petersen, N. O. 1984. Diffusion and aggregation in biological membranes. *Can. J. Biochem. Cell Biol.* 62:1158–1166.

Petersen, N. O. 1986. Scanning fluorescence correlation spectroscopy. I. Theory and simulation of aggregation measurements. *Biophys. J.* 49:809–815.

Petersen, N. O., D. C. Johnson, and M. J. Schlesinger. 1986. Scanning fluorescence correlation spectroscopy. II. Application to virus glycoprotein aggregation. *Biophys. J.* 49:817–820.

Qian, H., and E. L. Elson. 1990. On the analysis of high order moments of fluorescence fluctuations. *Biophys. J.* 57:375–380.

Rönnstrand, L., L. Terracio, L. Claesson-Welsh, C. H. Heldin, and K. Rubin. 1988. Characterization of two monoclonal antibodies reactive with external domain of the platelet-derived growth factor receptor. *J. Biol. Chem.* 263:10429–10435.

Schlessinger, J. 1988. Signal transduction by allosteric receptor oligomerization. *Trends Biochem. Sci.* 13:443–447.

Schlessinger, J., Y. Shechter, M. C. Willingham, and I. Pastan. 1978. Direct visualization of binding, aggregation, and internalization of insulin and epidermal growth factor on living fibroblastic cells. *Biochemistry.* 75: 2659–2663.

Schneider, M. B., and W. W. Webb. 1981. Measurement of submicron laser beam radii. *Appl. Optics.* 20:1382–1388.

Schreiber, A. B., J. Hoebke, B. Vray, and A. D. Strosber. 1980. Evidence for reversible microclustering of lentil lectin membrane receptors on HeLa cells. *FEBS Lett.* 111:303–306.

St-Pierre, P. R., and N. O. Petersen. 1990. Relative ligand binding to small or large aggregates measured by scanning correlation spectroscopy. *Biophys. J.* 58:503–511.

St-Pierre, P. R., and N. O. Petersen. 1992. Average density and size of microclusters of epidermal growth factor receptors on A431 cells. *Biochemistry.* 31:2459–2463.

Van Belzen, N., P. J. Rijken, W. J. Hage, S. W. de Laat, A. J. Verkleij, and J. Boonstra. 1988. Direct visualization and quantitative analysis of epidermal growth factor-induced receptor clustering. *J. Cell. Physiol.* 134: 413–420.

Weissman, M. B. 1981. Fluctuation spectroscopy. *Annu. Rev. Phys. Chem.* 32:205–232.

Weissman, M., H. Schlindler, and G. Feher. 1976. Determination of molecular weights by fluctuation spectroscopy: application to DNA. *Proc. Natl. Acad. Sci. USA.* 73:2776–2780.

Yarden, Y., I. Harari, and J. Schlessinger. 1985. Purification of an active EGF receptor kinase with monoclonal antirecptor antibodies. *J. Biol. Chem.* 260:315–319.